ELSEVIER

High resolution radiant distribution and orbits of sporadic radar meteoroids

M.D. Campbell-Brown

Department of Physics and Astronomy, University of Western Ontario, London, ON, N6A 3K7, Canada

Abstract

Five years of meteor orbit data from CMOR (the Canadian Meteor Orbit Radar) are used to study the high-resolution orbital structure of the sporadic meteoroid complex. The large number of high quality orbits (2.35 million) allows the orbital characteristics of meteoroids to be studied not only in the five sporadic sources accessible from the latitude of London, Ontario, Canada, but at a resolution of 2 degrees. The radiant distribution of sporadic meteors is investigated, applying corrections for observing biases, and weighting to a constant limiting mass, and to a constant limiting energy. The orbital distribution of the sporadic sources is compared to other studies. The variation of average geocentric speed, semimajor axis, eccentricity, inclination and perihelion distance with meteoroid radiant is investigated. The source of a ring depleted in meteor radiants at 55 degrees from the apex is attributed to shorter collisional lifetimes inside the ring, due to a higher probability of catastrophic collisions with particles in the zodiacal cloud for the predominantly retrograde meteoroids inside the ring.

1. Introduction

Sporadic meteoroids are those which have evolved sufficiently from the orbit of their parent body that they are no longer easily linked to that parent, or to other meteoroids from the same parent. Earth-based observations are the only practical way to study sporadic meteoroids in the millimeter size range, since the spatial density is too low for space-based collectors, and meteoroids in this size range cannot be seen optically unless they collide with the Earth or another planet. In spite of the limitation this imposes, sampling the sporadic meteoroid complex at 1 AU provides a wealth of detail which can be used investigate the origins and evolution of the complex. In order to determine the distribution of Earth crossing meteoroids, any set of sporadic meteoroid orbits must be corrected for observing biases and collision probabilities with the Earth.

The sporadic meteoroid complex has been studied for many decades, and six principal apparent "sources," or directional enhancements, of meteor radiants have been identified. Note that the term "source" is applied to the radiant concentrations, but each consists of meteoroids from many true sources (parent bodies); for this reason, we will often refer to them as "apparent sources." These apparent sources have constant locations in a coordinate system which is centered on the apex of the Earth's way, and rotates as the Earth orbits the Sun. The helion and antihelion sources dominate in most studies, and were the first to be discovered in radar studies at Jodrell Bank and Adelaide (Hawkins, 1956; Weiss and Smith, 1960). They are located approximately 70 degrees from the apex, along the ecliptic; the helion source is thus 20 degrees from the direction of the Sun, and the antihelion 20 degrees from the anti-Sun point. The north and south apex sources (Sekanina, 1976) are located approximately 20 degrees north and south of the plane of the ecliptic, in the apex direction. The last apparent sources to be discovered were the north and south toroidal sources (Elford and Hawkins, 1964; Jones and Brown, 1993), located approximately 60 degrees to the north and south of the apex.

The orbital properties of the helion/antihelion and apex sources have been studied by radar before, using both transverse and head echo scattering. Transverse scatter radars observe mainly specular reflections from meteor trains; they usually employ broad beams. Head echo scatter radars observe mostly the radiation reflected from the cloud of ionization immediately

surrounding the head of the meteoroid; they tend to have antennas which direct the power in smaller beams.

The first study of apparent sporadic sources from individual radar orbits was done by Jones and Brown (1993), using data from the Harvard Meteor Radar Project (HRMP), a transverse scatter system. No corrections were applied to the data in this study, though the corrected orbital distribution of all the HRMP meteors was calculated by Taylor and Elford (1998).

The most notable orbit study to date is by Galligan and Baggaley (2005), using the Advanced Meteor Orbit Radar (AMOR). AMOR uses a fan shaped beam to detect transverse meteor echoes; an interferometer and two remote stations allow orbits to be computed. Galligan and Baggaley corrected a set of 5×10^5 orbits, taken over 5 years, for in-atmosphere observing biases and Earth-collision probabilities, and looked at the distributions of orbital parameters for the helion, antihelion, and apex sporadic sources. This study is certainly the most rigorous to date, taking into account attenuation due to initial radius, finite velocity, pulse repetition frequency and Faraday rotation. They also took into account daytime interference from ionospheric sporadic E-region echoes, and data down-time of the radar. Showers were removed, and hyperbolic orbits were excluded from the analysis.

A smaller study has been done with data from the Jicamarca Radio Observatory (JRO) (Chau et al., 2007), based on 1.7×10^5 orbits taken over 14 random days, spread over nearly six years. The JRO, with a narrow, $2°$ beam, is a head echo scattering radar. They looked at the simple radiant distribution, without correcting for in-atmosphere observing biases. The sample is predominantly (72%) retrograde meteoroids, due mainly to the high order dependence of head echo scattering cross-section on speed. This makes fast meteors much easier to detect. They observed all six apparent sporadic sources; the apex sources showed the most detail since the numbers were highest for those apparent sources. Both the northern and southern apex sources were roughly circular in shape, with a denser core which was narrow in ecliptic longitude, but having the full latitude extent of the circular source. The limiting size of meteors observed with the JRO has not been calculated.

In a recent study, the radiant distribution of sporadic meteors was investigated using CMOR (the Canadian Meteor Orbit Radar) (Campbell-Brown, 2007), a transverse scatter radar. In addition to the five apparent sources visible from the northern hemisphere, analysis of 2.35×10^6 orbits, taken over five years (from 2002 to 2007), showed a ring of enhanced sporadic activity centered about the apex, with an inner radius of approximately 55 degrees. Immediately inside the ring there were very few radiants. The cause of the ring appeared to be collisional: meteoroids just inside the ring had slightly enhanced probabilities of collision with the Earth.

In the present study, showers have been removed from the CMOR data set. We examine the radiant distribution at $2°$ resolution in raw form, corrected for atmospheric observing biases, weighted to a uniform limiting mass, weighted to a uniform limiting energy, and corrected for collisional probability with the Earth. We also examine the raw orbital distribution at uniform limiting radar magnitude, and look to the collisional life-times of meteoroids to explain the ring feature in the sporadic distribution.

2. Observations

CMOR, located in Ontario, Canada at 43.264 N, 80.772 W, has been operating in its current form since 2002; it is described in detail in Jones et al. (2005). This study uses only one of the three frequency systems: the 29 MHz system, which is the only one with orbital capabilities. Two remote stations, 6 and 8 km away from the main radar site, have receivers, from which the data is transmitted to the main site over microwave links. The time differences between echoes received at the main site and each of the two remote sites, along with the directional information from an interferometer at the main site, allow a meteor's trajectory to be calculated. In particular, the radiant and speed of the meteor can be used to find the meteoroid's orbit. The radar has a limiting mass at 30 km/s of 10^{-7} kg.

Since the echoes considered here are produced by specular scattering from the ionized meteor train, echoes received at the main station may not be received at the two remote sites. Scattering to the remote sites takes place a few km along the trail from the main site echo (hence the time delays among the echoes); if the trail does not extend far enough in the right direction, no echo will be received. Roughly thirty percent of echoes received at the main station are also seen at the two remote sites.

CMOR uses one 3-element yagi antenna to transmit at 29 MHz, and uses 2-element yagis to receive. This arrangement produces a very broad gain pattern, covering the whole sky down to 20 degrees elevation. The broad radiation pattern allows some meteors from all radiants to be observed nearly all the time those radiants are above the horizon, and is therefore ideal for surveys of sporadic meteors.

Several million 3-station echoes from single meteors have been recorded since 2002. This initial dataset has been carefully examined, looking particularly for errors in the interferometry. Meteors with heliocentric speeds more than 100 km/s were rejected (these being entirely due to errors in the time determinations from the remote sites), which was only 1% of the data set. Interferometry was done independently on each echo using two different methods (see Jones et al., 1998), and only those that agreed to within $1°$ were kept. Following this analysis, 2.35×10^6 orbits were selected; it is expected that this subset represents properly determined orbits with few erroneous orbits due to interferometry or echo timing errors. These orbits are well distributed in solar longitude: in any 10 degree solar longitude interval, there are at least 4×10^4 orbits, up to nearly 1×10^5 for some intervals. The time variation of the rates and orbital parameters will be examined in a future paper.

3. High resolution radiant distribution

For each orbit, the heliocentric ecliptic latitude and longitude (λ and β) of the radiant were calculated, corrected for zenithal attraction, diurnal aberration and gravity acceleration. To keep the directions constant with respect to the Earth, the solar longitude of the Earth at the time of observation (λ_0) was
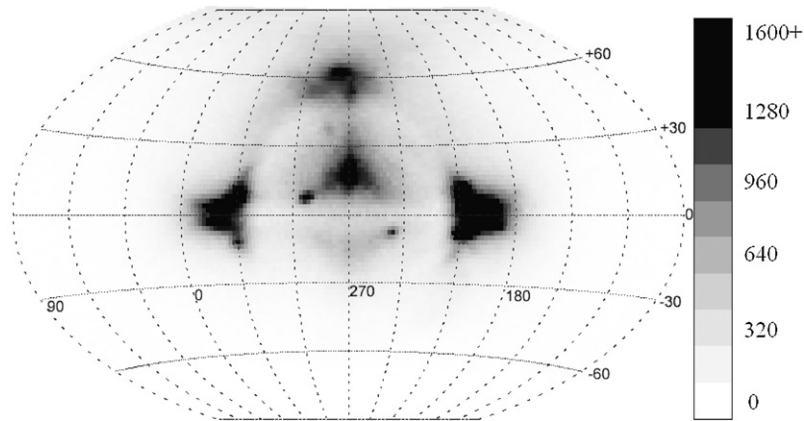
Fig. 1. Raw radiant distribution of all CMOR orbits, in 2° bins, in heliocentric coordinates. The helion source is to the left, the north and south apex sources in the center, the antihelion source to the right, and the north toroidal source near the top of the plot. The scale represents the number of individual radiant determinations in each 2 × 2 degree bin.
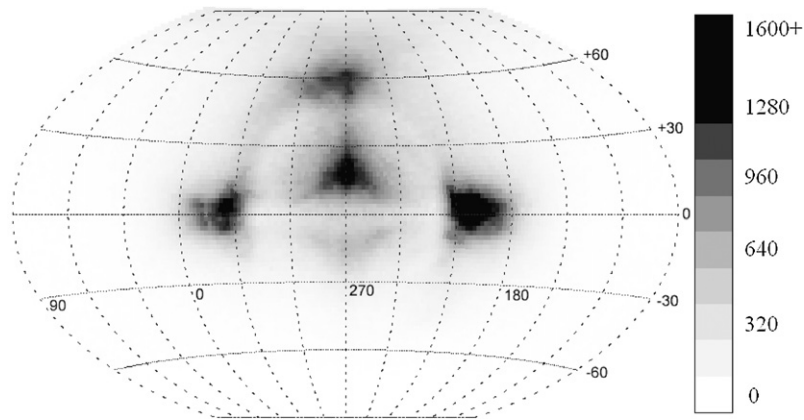

Fig. 2. Raw radiant distribution of sporadic CMOR orbits, after removal of 45 showers.

subtracted from the ecliptic longitude, making the coordinates Sun-centered. The celestial sphere was divided into bins two degrees in latitude and in longitude; 90 bins total in latitude, and between 180 (at the ecliptic) and 1 (at the pole) bins in longitude. The distribution of all 2.35×10^6 orbits is shown in Fig. 1. Note that we place 270° heliocentric longitude in the center of the plot to keep the presentation clear. The ring dividing the region of excess radiants from the region depleted in radiants is clearly visible. The north toroidal source, and the inner edges of the helion and antihelion sources, protrude into the region of depleted radiants.

Several strong meteor showers are obvious in Fig. 1, including the Perseids (just above and to the left of the north apex source), Eta Aquariids (at the bottom left of the north apex) and the Orionids (to the right of the south apex source). Other strong showers, like the Arietids and Geminids, fall within the helion and antihelion sources and are not clearly distinguishable. In order to examine the sporadic distributions without shower contamination, 45 major meteor showers (listed in Brown et al., 2008) were removed from the data. On days when the showers were active, all echoes within 5 degrees of the radiant and 10 km/s of the catalogued atmospheric speed of the shower were excluded from the analysis. This left 2.21×10^6 orbits, or 94% of the original data set. The raw radiant distribution of this

subset is shown in Fig. 2. The showers near the apex sources are now gone, and the helion and antihelion sources have lost some of their structure. Helion and antihelion showers tend to extend along the ring structure; their removal makes the sources rounder.

The next step is to correct for the atmospheric observing biases of the radar. The first correction is for the radar's collecting area. The integrated daily collecting area for a particular radiant depends only on that radiant's declination: radiants near the north pole have the highest collecting areas, and southerly radiants the least. For each meteor, the integrated collecting area was calculated, and the echo was scaled accordingly. This correction increases the activity of the radiants below the north ecliptic pole (where the collecting area is maximum), with the highest correction to the south apex source, though the latter is still smaller than the north apex source due to the observing geometry. If no echoes are seen from a south apex radiant, no correction factor can be applied.

Each of the atmospheric effects discussed below were calculated using the formalism in Ceplecha et al. (1998). The most important atmospheric bias, for the CMOR radar, is the initial trail radius effect. Faster meteors, which ablate higher in the atmosphere, produce larger diameter trains because of the increase in mean free path with altitude. When the transverse
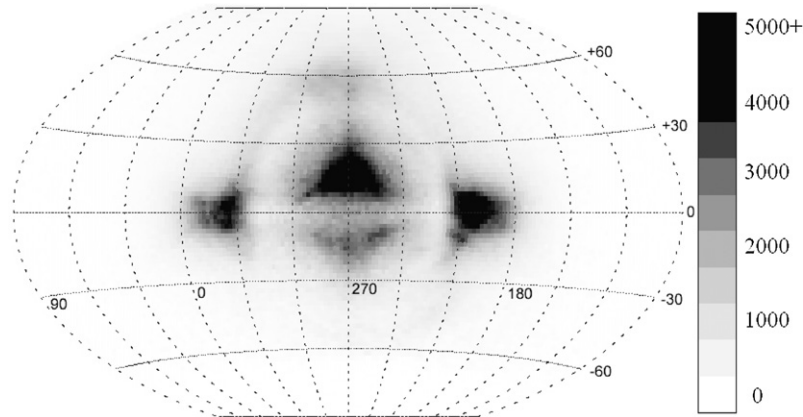
Fig. 3. Radiant distribution of sporadic CMOR orbits, corrected for in-atmosphere observing biases.

spread of the trail is of order the radar wavelength, destructive interference between the front and the back of the trail reduces the amplitude of the echo, making it less likely to be observed. This affects only underdense echoes; since the meteor detection software on CMOR rejects overdense echoes, the entire data set is affected. The attenuation of each meteor due to initial radius was estimated from the height and speed, and this was used to scale the orbit to account for similar meteors missed because of initial radius. For example, if the probability of observing a particular meteor was 50% because of observing biases, the meteor would be counted twice. This correction factor increases the activity of the apex sources, which contain the fastest meteors and are therefore most attenuated by initial radius. The nature and magnitude of the initial radius correction remains somewhat uncertain and this uncertainty represents the largest potential systematic error in the present study.

We have also calculated the Faraday rotation (in which the radar wave's polarization is rotated while passing through ionization, attenuating the received echo) of each meteor using a model ionosphere. Since the ionospheric density below 100 km (where most of CMOR's echoes occur) is significant only during the day, Faraday rotation affects mainly the helion source. Even after this correction, the helion source is not as strong as the antihelion source. Since orbits of meteoroids in the two apparent sources are part of the same population, it seems reasonable to expect the average strength of the two sources to be the same. The difference may be due to other ionospheric effects.

The final two effects for which correction factors were generated are the finite velocity effect and the pulse repetition factor. In the former, expansion of the ionized meteor trail while the meteor is crossing the first Fresnel scattering zone may cause attenuation on top of the initial radius factor. This affects mostly slow meteors, and is not a major effect in our data; we see over 90% of echoes everywhere except some parts of the antapex. The pulse repetition factor (CMOR has a PRF of 532 Hz) takes into account echoes which may be missed because they decayed rapidly, before enough radar pulses could scatter off them to identify them as meteors. It is also a minor effect for CMOR, affecting the apex region most strongly; even there it is estimated that over 90% of echoes are seen.

If the total scaling factor for any orbit was more than 30, meaning we would expect 29 similar meteors to have been missed due to observing biases (usually because of very small collecting areas), the orbit was discarded. This arbitrary limit was imposed to prevent very large fluctuations in the distribution produced by a small number of heavily biased observations. Because of the stringent quality tests at the outset, only 0.6% of the data set was lost at this step. The distribution of echoes corrected for atmospheric effects is shown in Fig. 3.

The previous step gives a true distribution of meteoroids at the top of the Earth's atmosphere, but to a limiting ionization value, or radar magnitude. Faster meteoroids will produce more ionization per unit mass than slower meteoroids, and so the limiting mass for fast meteors is smaller than for slower meteors. If we wish to see what the distribution of meteoroids looks like at some constant limiting mass, we must account for this effect. Bronshten (1983) found, after an extensive literature review, that meteor ionization was proportional to $v^{3.42}$; we use $v^{3.5}$ here for simplicity. Each meteor was given a scaling factor to adjust it to the limiting mass at 30 km/s; slower meteors have a correction factor greater than one, faster meteors have correction factors less than one. The corrected, mass weighted distribution is shown in Fig. 4.

This step shows that the strength of the north and south apex and the north toroidal sources is in small meteoroids. The only apparent sources that remain after the mass weighting step are the helion and antihelion.

The fact that the north and south apex, and the north toroidal sources are not visible in the mass weighted plot does not mean that these sources are artifacts; they are actual radiant concentrations that contain smaller particles. The relative importance of each apparent source depends on what aspect of the meteoroids is of interest. To illustrate this, we have corrected the sporadic distribution to a constant limiting energy, instead of mass, by applying a v^2 term. This may be of interest in judging the physical damage a meteoroid would do to a spacecraft in a collision (neglecting plasma effects). The results are shown in Fig 5: the apex sources are reduced from the ionization weighted plot, but they are still significant compared to the helion and antihelion sources.
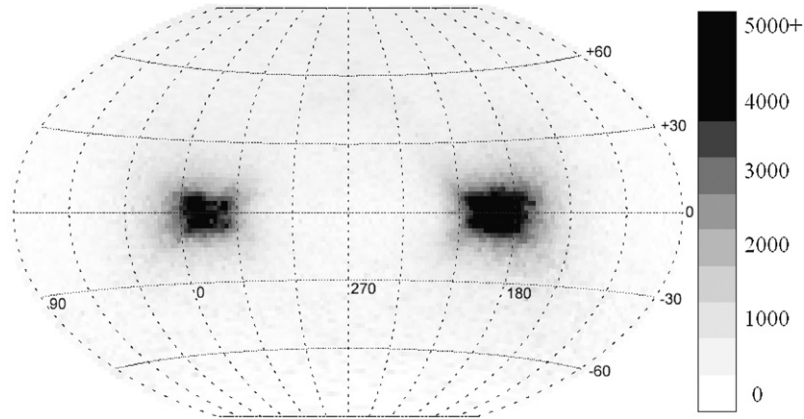
Fig. 4. Radiant distribution of sporadic CMOR orbits, corrected for in-atmosphere observing biases and weighted to a uniform limiting mass.
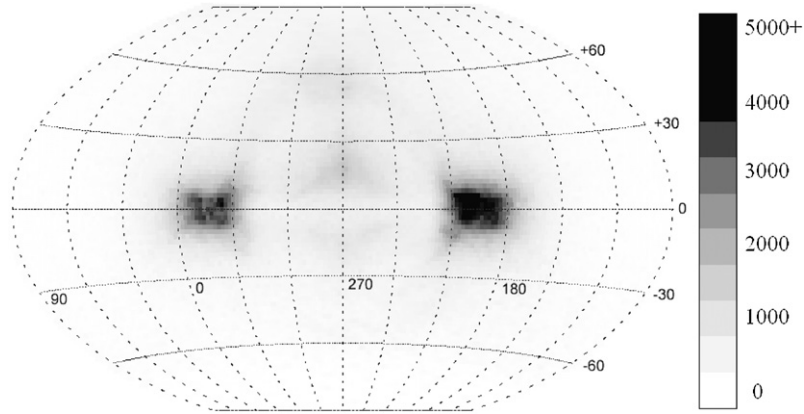

Fig. 5. Radiant distribution of sporadic CMOR orbits, corrected for in-atmosphere observing biases and weighted to a uniform limiting energy.

It is also useful to look at the distribution of radiants after correcting for the probability of collision with the Earth, using Öpik's formalism as cited in Galligan and Baggaley (2004):

$$n_c \sim \frac{v_\infty^2}{v_g^2 a^{1.5} \sin i} \sqrt{\frac{3 - a^{-1} - 2\sqrt{a(1 - e^2)} \cos i}{2 - a^{-1} - a(1 - e^2)}}. \qquad (1)$$

Here v_∞ is the meteoroid speed at the top of the atmosphere, without deceleration. Under certain conditions, the collision probability becomes infinite (an inclination of 0, for example, will produce this result); we dealt with this by setting the collision probability to 100 in such cases. The log of the collision probability is shown in Fig. 6. Each meteor radiant was individually corrected, after its collision probability had been calculated; the results are shown in Fig. 7. The main effect is to remove radiants on the ecliptic, which are very likely to collide with the Earth.

4. Comparison with previous studies

4.1. Positions and relative strengths of the apparent sporadic sources

We can compare the relative strengths of the apparent sporadic sources and their positions with other data. To find the positions and strengths, we have fitted a gaussoid function to each of the five sources, in the raw and the corrected data. This gives the relative activity, longitudinal and latitudinal width and position for each of the five apparent sources. The five uncorrected apparent sources are shown in Fig. 8; the positions and widths of the apparent sources (raw, and after bias corrections and weighting to a common limiting mass) are given in Table 1. For comparison, we have AMOR data from Galligan and Baggaley (2005), both raw and corrected; data from Brown and Jones (1995), who used raw data from Harvard and other radars to calculate positions and data from the Springhill and Christchurch radars gathered in the 1960s to calculate the corrected flux of each of the apparent sporadic sources; and raw positions and strengths from JRO (Chau et al., 2007).

In the raw CMOR data, the antihelion source is by far the strongest, with the helion and north apex having similar strengths. The AMOR data shows a similar antihelion strength, but the helion source is a smaller fraction of the antihelion strength (approximately 60%, compared to approximately 75% for CMOR). The sum of the apex sources [Galligan and Baggaley (2005) do not separate the north and south apex] is much greater in the raw AMOR data than the raw CMOR data. Galligan and Baggaley (2005) did not compute the strength or position of the south toroidal source. Chau et al. (2007) found data dominated by the apex source, but this is due to the severe speed dependence of the radar scatter. The relative strengths of
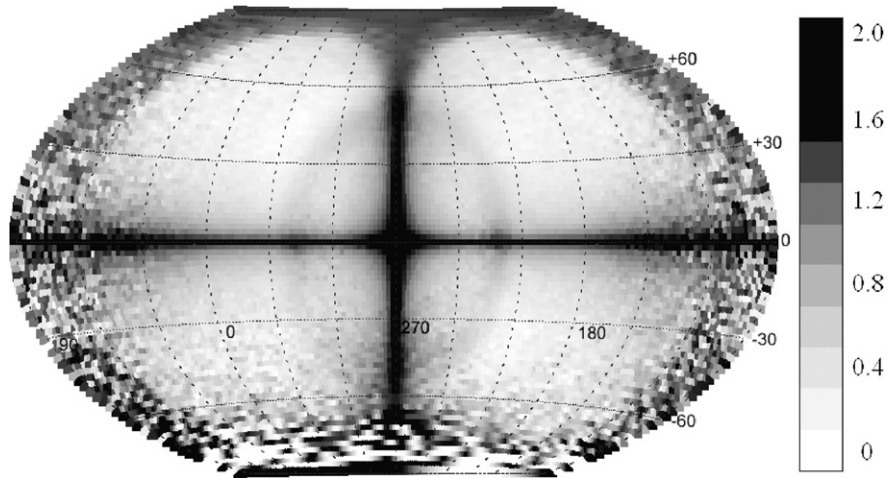
Fig. 6. Log of the average collision probability of meteors, by 2° bins in heliocentric coordinates.
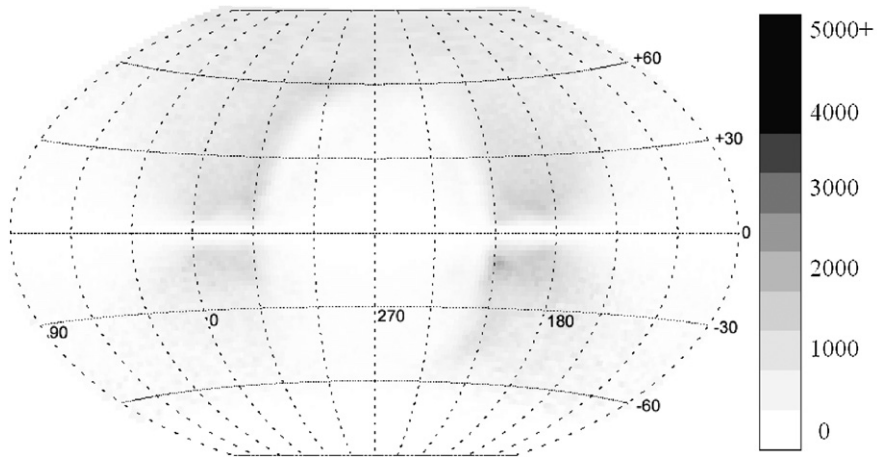

Fig. 7. Radiant distribution of sporadic CMOR orbits, corrected as in Fig. 4 for in-atmosphere observing biases and weighted to a uniform limiting mass. This figure is additionally corrected for collision probability with the Earth.
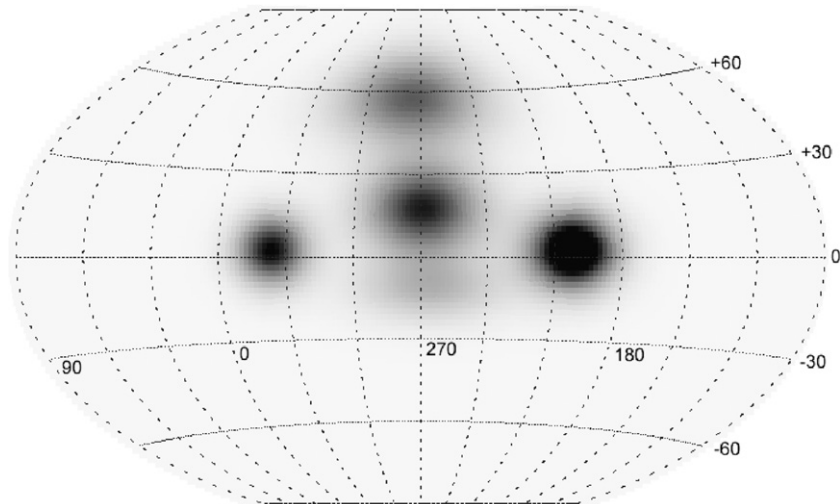

Fig. 8. Gaussoid fits to the five apparent sporadic sources seen by CMOR, from uncorrected data.

Table 1
Relative strengths (in percent of total sporadic meteors), positions and widths for the apparent sporadic sources; raw data, and corrected to a constant limiting mass. CB = current study; GB05 = Galligan and Baggaley (2005); Ch07 = Chau et al. (2007); BJ95 = Brown and Jones (1995). Note that AMOR results are given only for a single apex source

	Source	Study	Rel. strength	$\lambda - \lambda_\odot$	β	λ width	β width
Raw data	Antihelion	CB	29	202	2.2	15	11
		GB05	27	205	−11	16	23
		Ch07	1	200	0	12	10
		BJ95		198	0	18	18
	Helion	CB	22	337	2.4	12	10
		GB05	16	335	−15	17	23
		Ch07	0.9	340	0	12	10
		BJ95		342	1	16	16
	North apex	CB	21	269	18	21	12
		Ch07	17.5	270.5	13	3	9
		BJ95		271	19	21	21
	South apex	CB	10	266	−12	25	9
		Ch07	20.9	270	−13	3	9
		BJ95		273	−11	−	−
	Apex	GB05	52	270	−10	17	16
	North toroidal	CB	18	276	57	15	9
		Ch07	0.3	270	55	15	10
		BJ95		271	58	19	19
	South toroidal	Ch07	1.3	270	−55	15	10
		BJ95		274	−60	16	16
Corrected	Antihelion	CB	37	196	0.2	15	10
		GB05	40	200	−11	18	24
		BJ95	33				
	Helion	CB	31	342	0.2	15	10
		GB05	31	340	−15	19	24
		BJ95	36				
	North apex	CB	11	270	18	21	12
		BJ95	4				
	South apex	CB	11	260	−32	19	12
		BJ95	15				
	Apex	GB05	23	272	−10	19	16
	North toroidal	CB	10	275	56	13	9
		BJ95	6				
	South toroidal	BJ95	6				

the north and south apex sources depend strongly on the difference in collecting area between these regions, so the raw data is not useful for comparing their relative strengths—the helion and antihelion sources have the same average declination over a year as seen from any given latitude.

At a constant limiting mass, the antihelion and helion sources make up 68% of the sporadic source activity measured by CMOR, with the other three apparent sources being roughly equal. Even the correction for Faraday rotation does not make the helion and antihelion sources equal, though they are closer (the helion source is 84% of the antihelion). Similarly, the AMOR helion/antihelion ratio is closer to one after correction (77%), but there is still asymmetry. Interestingly, the Springhill/Christchurch data gives a slightly more active helion source: both of these single-station radars used crossed-dipole antennas which are not subject to Faraday rotation attenuation, which may partially explain the result. The total proportion of meteoroids in the helion/antihelion and apex sources agrees

quite well in the three studies, particularly those from AMOR and this study. The corrected north toroidal activity is much less than in the raw CMOR data, since the collecting area for this apparent source is high; the activity is still a higher percentage of the total than in the Springhill/Christchurch data.

The relative strengths of the apex sources are the same after correction of the CMOR data, though the error in the estimated strength of the south apex source is expected to be relatively large. Previous studies, including Brown and Jones (1995), have found that the south apex source is systematically stronger than the north apex source; they detail in that paper other studies which found the same thing. A difference in the average strength of these apparent sources is only possible if a significant number of the meteoroids in this population are less than one precession cycle away from their injection from their parent bodies to the population: otherwise the orbits would be distributed evenly. Our results suggest that the sources are

indeed balanced, but given our uncertainties, more study is warranted.

The positions of each of the apparent sporadic sources are similar in each of the studies, with the exception of the AMOR latitudes, which are all between 10 and 15 degrees below the ecliptic, for sources with expected symmetry about the ecliptic. The correction for collecting area in the CMOR data tends to bring the helion and antihelion sources closer to the ecliptic; they are expected to be symmetrical around the ecliptic, and their greater observed strength above the ecliptic is only due to the higher collecting area. A similar correction is not seen in the latitudes of the corrected AMOR data. The mass weighting correction moves the helion and antihelion sources further from the apex, toward the Sun and anti-Sun points, respectively, since orbits on the outsides of those apparent sources have lower speeds and therefore higher average masses. This is visible in both the CMOR and AMOR data.

The south apex source is not symmetric with the north apex in the CMOR data: again, this is due to the low collecting area in the southern part of the source which prevents a reliable set of orbits from being collected in this region. The south apex source shows a significantly different center in the mass weighted set: this is because of the small number and large corrections.

The apparent source widths vary greatly from study to study. This is particularly so in the width in latitude of the helion and antihelion sources (23 degrees from AMOR data, only 10 for JRO), and in the longitude width of the apex sources (3 degrees for JRO, 21 and 25 degrees for CMOR). Part of the latter difference is due to the fact that Chau et al. (2007) took the main apex source to be the narrow component, and the broader component is omitted in their width measurements. The widths of the apparent sources are not strongly affected by the corrections: the mass weighted widths in the CMOR data are different for the apex and toroidal sources, but in part this is because of the weakness of these sources in the corrected dataset, which introduces greater errors.

4.2. Orbit distributions

It is also interesting to compare the raw and corrected orbit distributions obtained in this work with those from previous studies of radar meteors. We have taken raw and corrected distributions from Galligan and Baggaley (2005), which give raw and corrected AMOR distributions for all sporadic meteors, and the helion/antihelion and apex sources. We also have raw data from the Harvard Radio Meteor Project (HRMP) for the helion/antihelion sources, the apex source and the north toroidal source (Jones and Brown, 1993), and corrected data for the whole data set (Taylor and Elford, 1998). We obtained the raw HRMP dataset from the IAU Meteor Data Center (Lindblad, 2001), and used this to calculate the raw orbit parameter distributions for the entire set as well. We did not have the information needed to correct the data for observing biases. We did not compare our data to the speed distributions for each sporadic source from JRO, given in Chau et al. (2007); only the raw distributions were given, and head echo radars have different observing biases from transverse scattering radars.

All three radar systems collected data with two or more outlying stations (the HRMP system had eight outlying receivers: see details in Cook et al., 1972), and so calculated orbits. The HRMP system, which collected 1.4×10^4 orbits during the 1960s, used a fan shaped beam, and ran at a frequency of 41 MHz. The radar had a limiting mass at 30 km/s of 10^{-7} kg, which is similar to the CMOR limiting mass at this speed. The bias corrections are described in detail in Taylor (1995) and Taylor and Elford (1998) (where the initial radius correction was added). They did not correct for Faraday rotation, the finite velocity effect, or the PRF effect. They assumed a dependence of ionization on v^4, and a mass distribution index $s = 2.1$.

The AMOR data set used for comparison here consists of approximately 5×10^5 orbits collected mainly in the 1990s. The AMOR system operates at 26 MHz, using a fan shaped beam. The limiting mass at 30 km/s is approximately 10^{-9} kg, so the particles seen by AMOR are considerably smaller than those in the HRMP or CMOR data sets. The bias corrections for this data set are described in Galligan and Baggaley (2004): they used the initial radius, Faraday rotation, finite velocity and PRF corrections as described in Ceplecha et al. (1998), as we have for the CMOR data set. They assumed ionization proportional to $v^{3.42}$, and a differential mass distribution index $s = 2.1$.

We obtained the distribution of all CMOR orbits by binning all of the raw echoes in each orbital parameter. From the raw distribution, it can be seen in Fig. 9 that the AMOR system sees more high speed, high inclination meteoroids than the CMOR system. Because of its slightly lower frequency, the AMOR system suffers less initial radius attenuation than CMOR; differences in the meteoroid population at the different mass ranges observed may also contribute to this effect. Harvard sees even fewer high speed, high inclination meteoroids than CMOR, which is consistent with the more severe initial radius effect expected because of its high frequency and the fact that it used fresnel speed measurements, not time-of-flight measurements as AMOR and CMOR do, meaning the data set is biased against fragmenting meteoroids, which are expected to predominate at the higher velocities where there is a higher proportion of cometary meteoroids. Interestingly, CMOR sees the most high eccentricity orbits, more than either AMOR or HRMP.

To obtain the corrected CMOR distributions, we applied a weighting factor to each orbit which included all the biases included in the previous section, with the weighting to a constant limiting mass; the corrected distributions are shown in Fig. 10. The corrected distributions for CMOR and AMOR look more similar, as we expect. The fact that the corrected distributions do not overlap may be due to true differences in the distribution of meteoroids in the two size regimes, as well as incomplete correction for observing biases. The AMOR system has significantly more high speed meteoroids than the CMOR system; the CMOR results show more very low speed meteoroids. The Harvard data produces a speed curve closer to the CMOR curve, with even more low speed meteoroids and fewer high speed. The inclination and eccentricity curves do not agree with CMOR or AMOR data, having more moderate prograde inclination meteoroids and more very eccentric orbits.
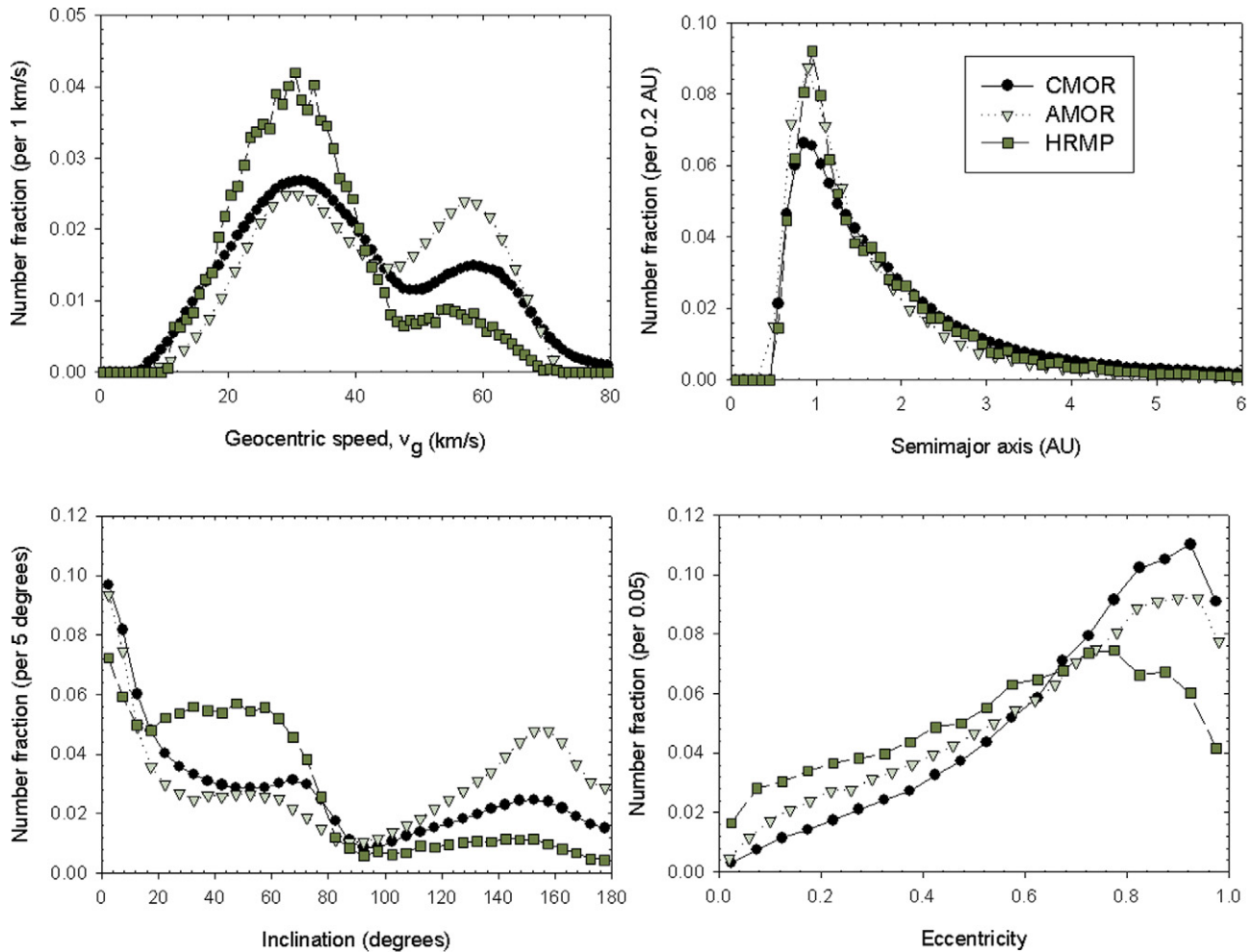
Fig. 9. Raw orbital parameter distributions for all orbits from CMOR (this work), AMOR (Galligan and Baggaley, 2005) and HRMP (from the raw data).

To obtain orbital distributions for each apparent sporadic source, we used the position and width of each apparent source as obtained in the previous section. We compare the raw distributions to those obtained with Harvard and AMOR, and the corrected distribution to AMOR. The raw source distributions for Harvard can be found in Jones and Brown (1993); all the AMOR source distributions are from Galligan and Baggaley (2005).

The raw distributions for the helion and antihelion sources are shown in Fig. 11. The three radars produce very similar curves for this apparent source, except in inclination; there the AMOR data set includes more prograde orbits with inclinations around 50 degrees. The helion and antihelion sources as measured by CMOR have very similar curves, as we expect.

Fig. 12 shows the corrected distributions for CMOR and AMOR. Here the excess of higher inclination orbits in the AMOR data set is increased, and there is also a notable excess of lower eccentricity orbits.

There is less agreement among radars when looking at the apex sources. Fig. 13 shows the CMOR, AMOR and Harvard distributions. The CMOR data set shows virtually no prograde, low geocentric speed meteoroids, while AMOR and Harvard (even more so) show significant numbers of prograde mete-

oroids. The Harvard eccentricity distribution is also very different from those of AMOR and CMOR, having an excess of high inclination meteoroids in the apex region. In the CMOR data set, the south apex source has higher speeds and inclinations than the north apex; we expect this since only the portion of the source close to the ecliptic (where geocentric speeds and inclinations are highest) is well sampled in the south apex source.

The raw AMOR distribution for the apex sources showed significantly more prograde apex members than CMOR. In the corrected distributions (Fig. 14), the situation is reversed: the mass weighting correction brings up the number of prograde, low geocentric speed meteoroids to be nearly comparable to the number of retrograde meteoroids. Analysis of CMOR data shows that these prograde meteoroids are largely seen by CMOR at the edges of the apex sources.

The raw and corrected distributions of north toroidal meteoroids are shown in Fig. 15, and compared with the raw distribution from Harvard. Galligan and Baggaley (2005) found that the south toroidal source was weak, and therefore did not examine the orbital distribution. Both raw distributions show nearly Gaussian distributions in speed and inclination, with CMOR seeing slightly higher speeds and inclinations. The raw eccentricity distribution found with CMOR data has significantly
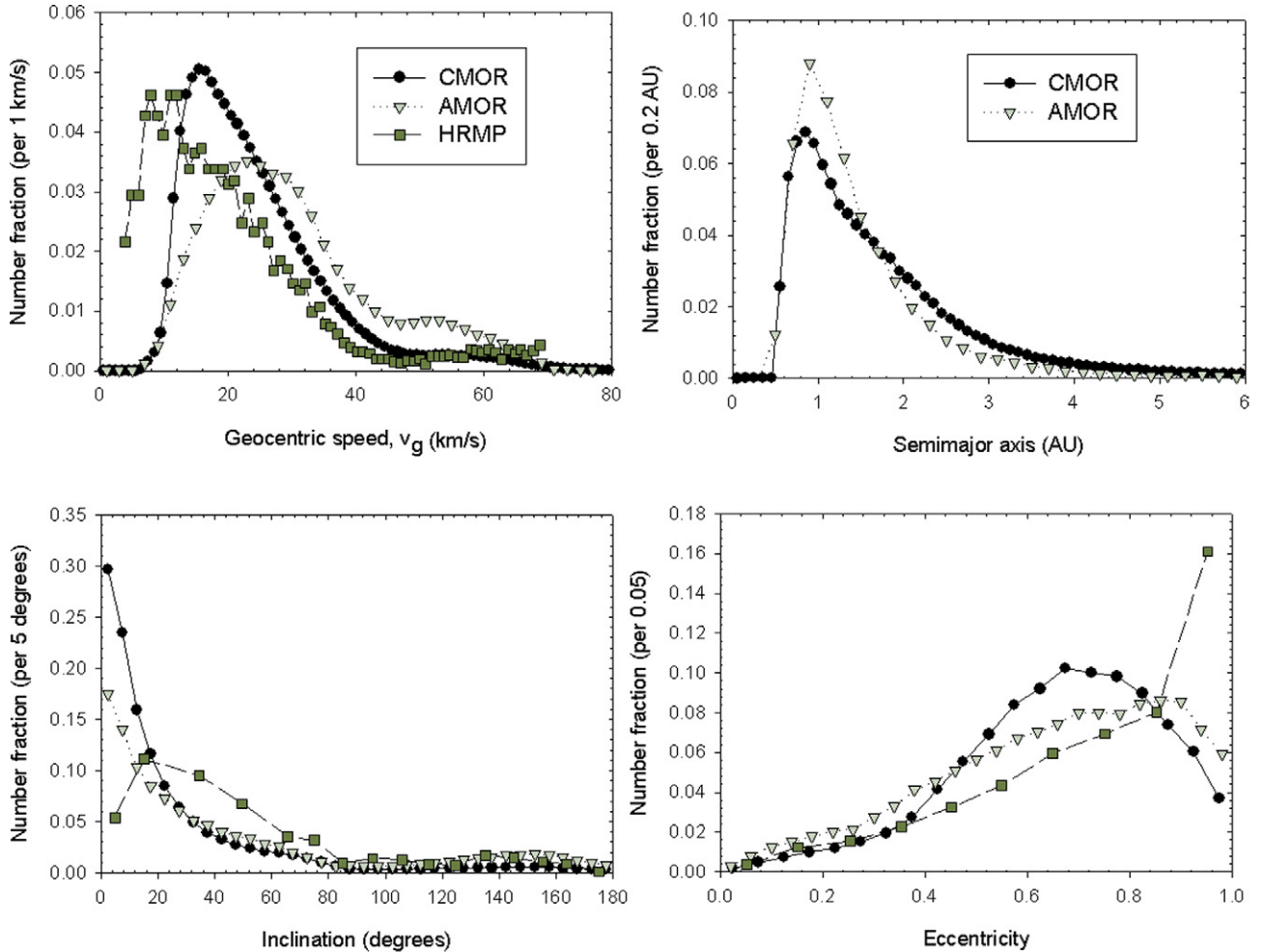
Fig. 10. Orbital parameter distributions for all orbits from CMOR (this work), AMOR (Galligan and Baggaley, 2005) and Harvard (Taylor and Elford, 1998), corrected for observing biases and mass weighted but not collision probability with the Earth. Note that Taylor and Elford (1998) did not calculate the corrected distribution of semimajor axis.

more high eccentricity meteoroids than that of Harvard. The mass weighted correction mainly brings out the low speed, low inclination component of the north toroidal source, and reduces the high eccentricity component. The fact that AMOR does not observe a strong south toroidal source may be due to a cutoff in the sizes of particles in this source.

5. Orbits

5.1. Orbital elements

In the past, the orbital distributions of the main apparent sporadic sources have been examined in aggregate: we wish to look at how orbital parameters vary across the sources, and outside the sources. We have chosen the simplest method for examining orbital parameters, which is to take the mean of the value in each radiant bin. It would be interesting to look at the actual distribution of orbits in each bin, but the amount of data then becomes prohibitive. Some more limited approach, looking at the distributions of a few selected regions, will be dealt with in a future paper.

We first examine the average speed of meteors in each radiant bin. Fig. 16 shows the average geocentric speed (v_g) for all meteors in each bin. To avoid weighting the distribution with anomalously high values of v_g, a cutoff speed of 80 km/s was imposed: values greater than this were rounded down to 80. Since the hyperbolic limit is around 72 km/s, this will tend to discriminate against unbound orbits; however, careful study of the CMOR data set (Weryk and Brown, 2004) has shown that virtually no orbits are conclusively hyperbolic. Most of the unbound orbits in our set are very eccentric orbits with some small error which has moved them into the unbound region.

As expected, the highest geocentric speeds are associated with meteors coming from the apex direction, where their heliocentric speeds add to the Earth's orbital speed. The ring structure is clearly visible as a local minimum in the speed (ranging from approximately 30 km/s on the ecliptic to approximately 40 km/s near the toroidal sources), moving away from the apex; like the boundary between the depleted zone and the excess of radiants in the radiant plots, this ring is located 55 degrees from the apex.

We can now look at the variation of speed with angular position across the apparent sporadic sources. The apex sources
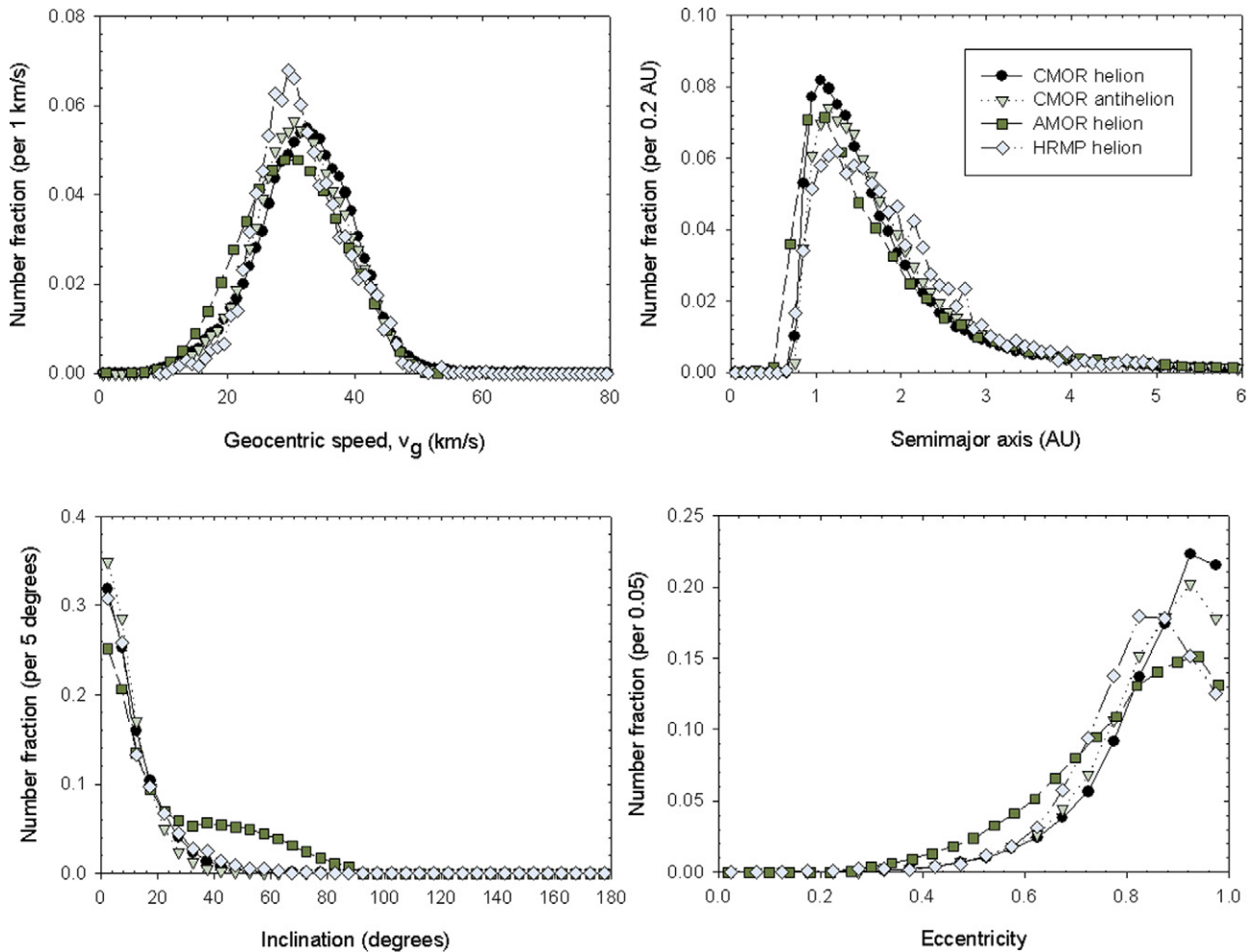
Fig. 11. Raw orbital parameter distributions for helion/antihelion sources from CMOR (this work), AMOR (Galligan and Baggaley, 2005) and Harvard (Jones and Brown, 1993).

have high speeds, which change very slightly from a maximum closest to the ecliptic (nearly 70 km/s) to slightly lower values at the north and south extremes (about 45 km/s). The speed distributions are very symmetric about the ecliptic, even though the rate plots are not. The helion and antihelion sources show the greatest variation, from approximately 20 km/s farthest from the apex, to 35 km/s closest to the apex. The north toroidal source is almost uniform, around 35 km/s.

It is worth examining other features of this plot, which will be important in all the plots of orbital parameters. First, the plot is very smooth in the regions of the apparent sporadic sources, where the number statistics are high; the plot becomes noisy near the antapex and low in the south, where very few orbits are detected. The second point is the southern limits of the system. CMOR can observe to radiant declinations 46.7 degrees south of the equator, since the radar is located at 43.3 degrees north, so the limiting southern ecliptic latitude is 70.1 degrees. Radiants from these ecliptic latitudes will only be observed for a small fraction of time, so the numbers are very small. However, there are measured geocentric radiants south of 70.1 degrees, all with low speeds. This can occur because very slow meteors coming from the south have their trajectories curved by the Earth's gravity, and strike the atmosphere from an apparent

radiant which is visible from northern latitudes. This zenithal attraction is taken into account in the radiant calculations. Finally, note that the apparent sporadic sources are not obvious in the speed plots as regions with distinct speeds. While the sources are identifiable in some plots of orbital parameters, in many plots the orbital parameters depend only on the radiant position, and not on whether the radiant is part of a source or not.

While the south toroidal source is not visible in the rate plots, a few south toroidal meteors are observed by CMOR. Although much noisier than the north toroidal source, the south toroidal source has nearly identical orbital properties.

The average semimajor axis, a, of CMOR meteors is shown in Fig. 17. Again, to avoid biasing the sample with very high or negative a's (for highly eccentric orbits, a small error in the speed produces a very large error in the semimajor axis), the a's were limited to 10 AU. The most prominent feature is the ring which was depleted in meteors in the rate plots: it consists of orbits with very low a's, close to 1 AU. The triangular north and south apex sources are visible as regions with low semimajor axes, with an even lower central core corresponding to the "narrow" component of these sources observed by JRO. The north toroidal source protrudes into the depleted region, vary-
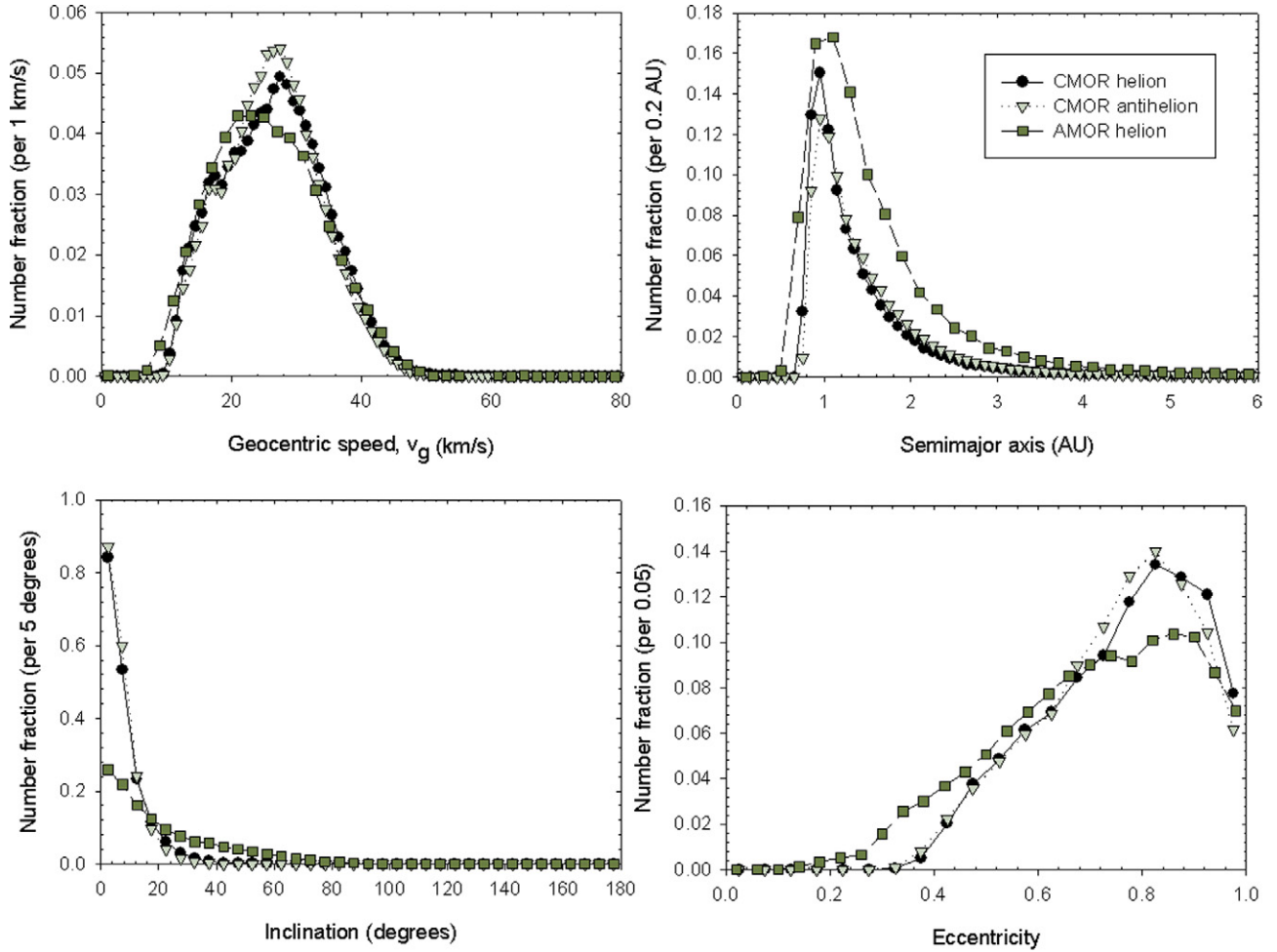
Fig. 12. Orbital parameter distributions for helion/antihelion sources from CMOR (this work) and AMOR (Galligan and Baggaley, 2005), corrected for observing biases and mass weighted, but not corrected for collision probability.

ing from orbits with reasonably large semimajor axes (around 7 AU) to small (around 3 or 4 AU) on the ring. The helion and antihelion sources are also clearly visible as regions of low semimajor axis to either side of the ring. Meteoroids from the antapex region tend to have very large semimajor axes. This is in part an observing bias of the radar: if the orbit of a meteoroid is only slightly larger than the Earth, the encounter speed in a collision with the back of the Earth will be low. Since slower meteors produce much less ionization, these meteors are much less likely to be observed than meteoroids on more eccentric orbits, which have higher encounter speeds.

Fig. 18 shows the average eccentricity, e, of the orbits. Again, orbits with eccentricities greater than unity were assigned an eccentricity of 1 to avoid skewing the average. The ring structure is again clearly visible, but the eccentricity on the ring changes from close to 0 in the north and south to nearly 1 at the ecliptic. The north toroidal source includes a region of low e on the ring, and the slightly larger e values outside. The narrow apex sources are very prominent in this plot, having much lower eccentricities than the broader source (0.1 compared to 0.6). The helion and antihelion sources are high eccentricity but also show variation over their extent, from 0.7 to nearly 1 going

toward the apex. Antapex meteors tend to have high eccentricities, corresponding to their higher semimajor axes.

The inclination of meteoroid orbits, i (Fig. 19), is strongly dependent on the heliocentric radiant, especially elongation from the apex. Meteoroids closer than 45° to the apex tend to be overwhelmingly retrograde, while orbits outside this ring are prograde. The inclination of meteoroids in the apex sources increases smoothly from nearly 180 close to the ecliptic to 110 at the northern and southern limits of the sources. The north toroidal source consists of meteoroids with uniformly high inclination, prograde orbits ($i \approx 70°$). The helion and antihelion consist of very low inclination, prograde orbits. It is worth emphasizing that the distribution of inclinations is determined by geometry: meteoroids with a given inclination are constrained to hit the Earth within certain regions. For example, an orbit with an inclination of 0 or 180 degrees must have a radiant on the ecliptic plane; whether they strike near the apex depends on whether the Earth has a higher or lower orbital speed at the time of encounter. An orbit with an inclination of 90 degrees and a particular longitude of perihelion is constrained to strike the Earth so that its apparent radiant falls on a circle about the apex, with the angular radius of the circle
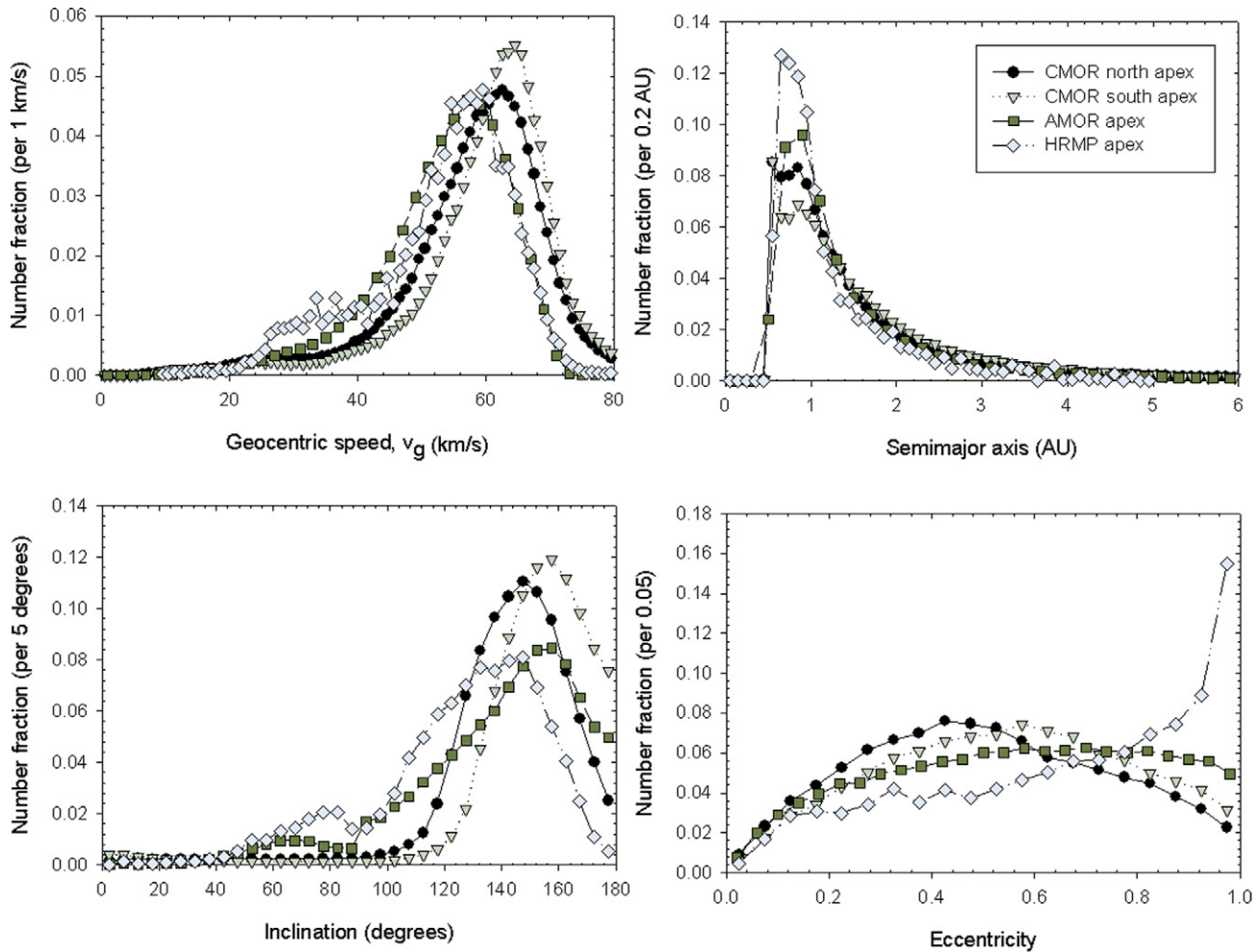
Fig. 13. Raw orbital parameter distributions for apex sources from CMOR (this work), AMOR (Galligan and Baggaley, 2005) and Harvard (Jones and Brown, 1993).

determined by the meteoroid's speed at the time of the encounter.

It is interesting at this point to see what fraction of echoes are prograde near the apex region. Galligan and Baggaley (2005) found that 4% of AMOR meteors were both prograde and part of the apex sources. Figs. 20 and 21 show the distribution of prograde and retrograde orbits, respectively. Less than 6% of prograde orbits are closer than 45 degrees to the apex; likewise only 7% of retrograde meteoroids have radiants outside of 45° from the apex. In both the prograde and retrograde case, the maximum number occurs on the 45° ring, and decays going inward and outward, respectively. There is no prograde apex source as such: what prograde orbits are measured in the apex region are the tail of a distribution outside the apex region.

The plot of perihelion distances (q), shown in Fig. 22, shows mainly geometric effects. Meteoroids with small q values tend to have radiants in the helion and antihelion directions, moved slightly toward the apex, since these very eccentric orbits are much more likely to be moving at angles approaching 90 degrees to the Earth's motion when they cross the Earth's orbit. The helion and antihelion sources are mainly composed of meteoroids with very small perihelion distances, increasing to about 0.5 AU on the inner edges. The perihelia of the apex

sources vary from about 0.9 AU on the line joining the apex to the pole to 0.5 AU at the east and west edges of the apparent sources. The north toroidal source is composed uniformly of particles with perihelia near 1 AU.

5.2. Meteoroid lifetimes

The reason for the ring which is depleted in meteoroids most likely lies in the collisional lifetimes of the meteoroids. We have already seen that meteoroids in this ring have a slightly elevated probability of striking the Earth; we want to look at their lifetimes considering collisions with other Solar System bodies, notably in the zodiacal cloud. We need a measure of the collisional lifetime which depends on the orbital parameters of the meteoroid: semimajor axis, eccentricity and inclination will all be important in determining the lifetime, since those will determine how much time the meteoroid spends in the zodiacal cloud and the encounter speed (which determines the energy of the collision, and therefore whether a meteoroid will be destroyed in a given collision). Steel and Elford (1986) have calculated the lifetimes of meteoroids of radius 1 mm with various a, e and i against catastrophic collisions with zodiacal dust particles, using a simple fan model for the zodiacal cloud. We fitted
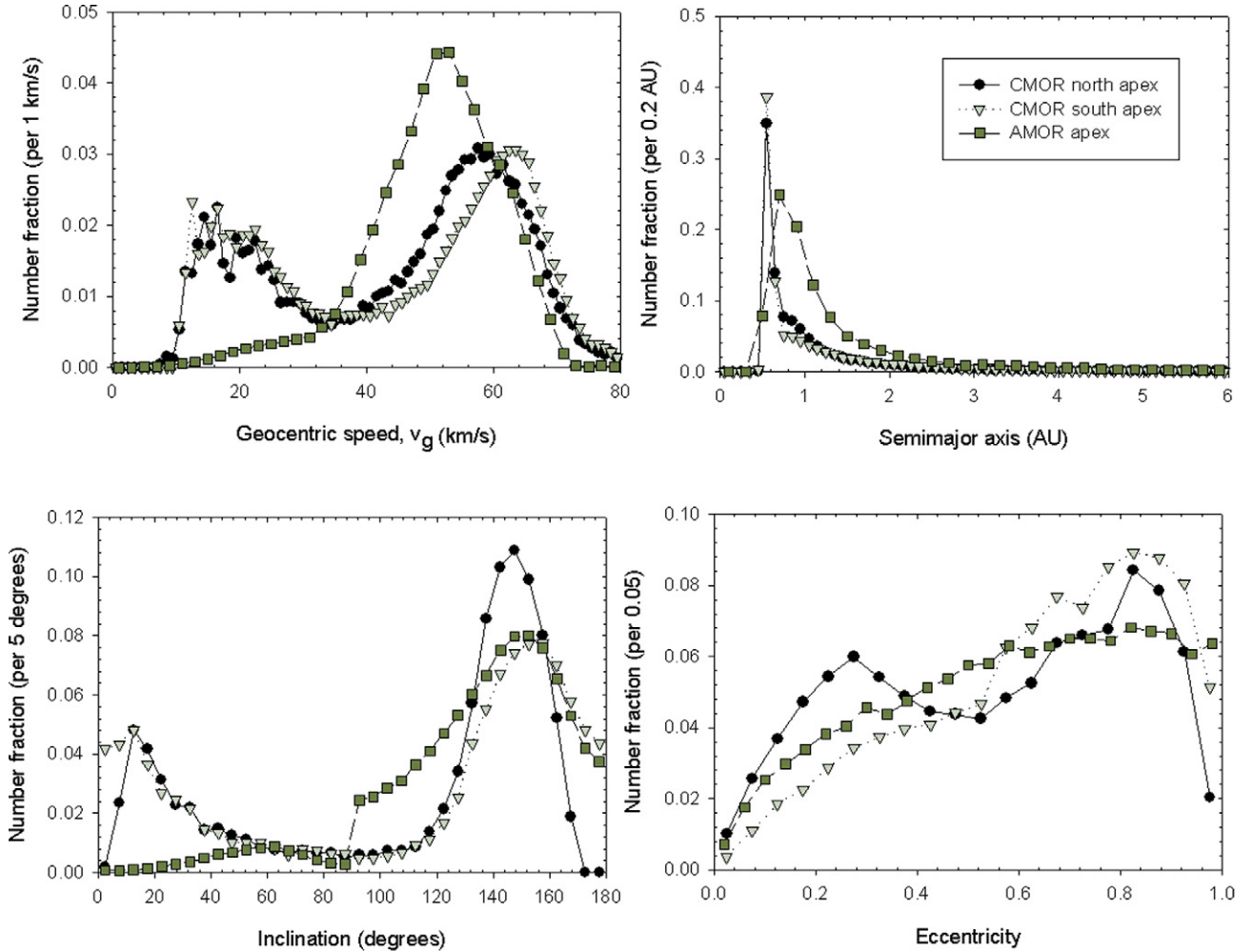
Fig. 14. Orbital parameter distributions for apex sources from CMOR (this work) and AMOR (Galligan and Baggaley, 2005), corrected for observing biases and mass weighted but not corrected for collision probability.

functions to the plots in their paper to obtain collisional lifetimes for any combination of a, e and i; the fits agreed with all provided plots to better than 5%. Collisional lifetimes were calculated for each CMOR orbit; the average lifetimes are plotted in Fig. 23.

The ring is the most prominent feature on the plot, having relatively short collisional lifetimes. The lifetimes are also short inside the ring, implying that the apex source must be replenished constantly. The helion and antihelion sources likewise consist of meteoroids with relatively short lifetimes, so they must be constantly replenished by their supply of meteoroids on timescales of order 10^4 years in order to remain the dominant apparent sources. The north toroidal source, other than a small band in its southern region, has relatively high collisional lifetimes, so the influx of particles need not be as high as the apex or helion/antihelion sources. Note the collisional lifetimes are an average of those particles which have survived to strike the Earth.

To see whether collisional lifetimes are the limiting factor for most of these meteoroids, we also calculated the average Poynting–Robertson lifetime for each radiant bin, using the formula in Olsson-Steel (1986) for meteoroids of size 1 mm and

assuming a meteoroid density of 1000 kg m^{-3}. The results are shown in Fig. 24. This plot shows clearly that the PR lifetime is strongly related to perihelion distance: meteoroids with small perihelia have the shortest lifetimes, since radiation effects are so much stronger for orbits which approach the Sun closely. The lifetimes are longer than collisional in all but a few scattered cases: to compare collisional lifetimes to PR lifetimes, we have plotted the ratio of the two in Fig. 25.

The collisional lifetimes are shorter than the Poynting–Robertson lifetimes on the ring, but nearly the same just inside and outside. At the apex and antapex, the collisional lifetimes are much (at least one order of magnitude) shorter, so collisional effects dominate over radiation effects. This emphasizes that for meteoroids encountered at the Earth both PR and collisional processes need to be taken into account in modeling efforts.

5.3. Correlations among orbital parameters

We can also look at the distribution of semimajor axis, eccentricity and inclination with respect to each other. Fig. 26 shows the raw distributions, the mass weighted distributions
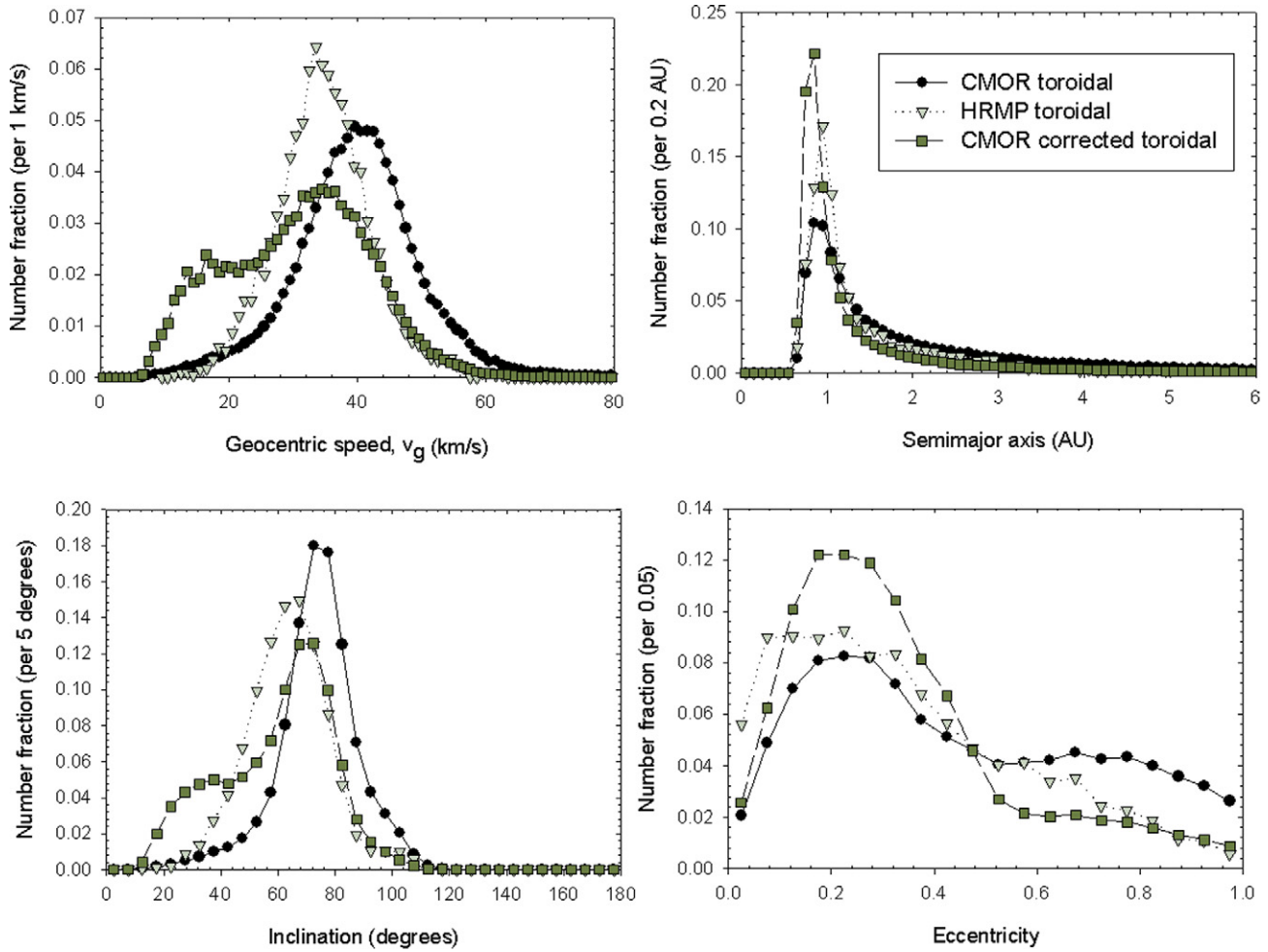
Fig. 15. Raw orbital parameter distributions for the north toroidal source from CMOR (this work) and Harvard (Jones and Brown, 1993). CMOR corrected distributions are also given.
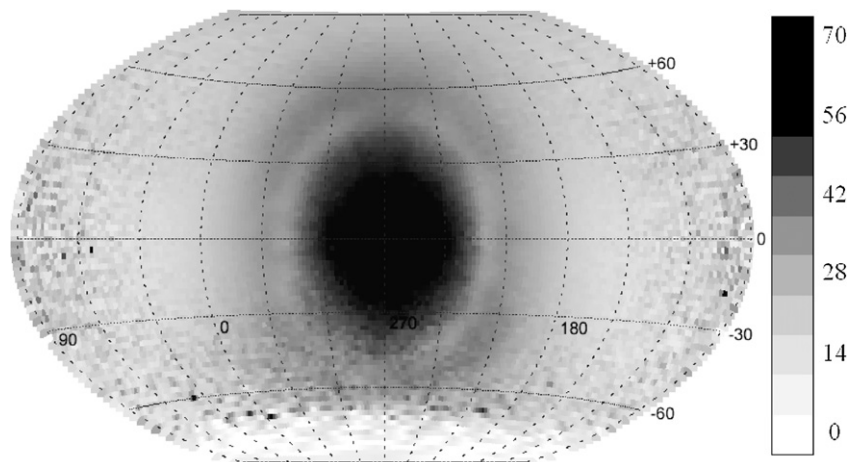

Fig. 16. Geocentric speed of meteors, in km/s, as a function of ecliptic latitude and Sun-centered longitude.

(with observing bias corrections) and the mass weighted, corrected distributions after correction for probability of collision with the Earth. Because all of the meteoroids were observed at 1 AU, their orbits are constrained to a particular region on the *a*–*e* plot.

The raw distributions shown here are similar to those of the HRMP data set and other meteoroid orbit surveys; see Steel (1996) for the orbital plots. The majority of raw orbits observed are prograde, with a noticeable dip in the numbers at inclinations around 90 degrees. It is possible to separate "comet-

Fig. 17. Semimajor axis of CMOR echoes, in AU.

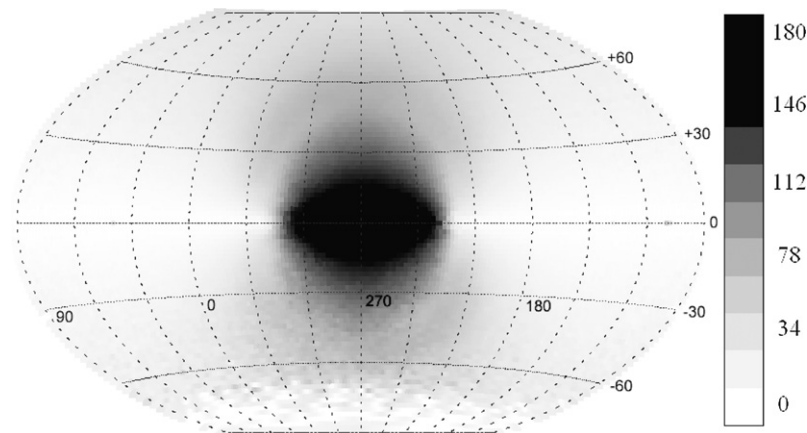Fig. 18. Eccentricity of CMOR meteors.

Fig. 19. Inclination of CMOR meteors, in degrees.

like" orbits from "asteroid-like" orbits using the K-criterion in terms of an object's a and e, but this is of limited usefulness in looking at meteoroids. Poynting–Robertson drag will tend to reduce the eccentricity of cometary objects, drawing them into the asteroidal region; north toroidal meteoroids, for example, have low eccentricities but high inclinations, and are almost certainly cometary in origin. From the asteroidal side, orbital evolution through resonances can result in orbits with

high eccentricities (Morbidelli and Gladman, 1998), putting those meteoroids in the cometary region of orbit parameter space.

6. Discussion

The first thing we hope to determine from a study of sporadic meteors is their origin. In particular, we want to know what the
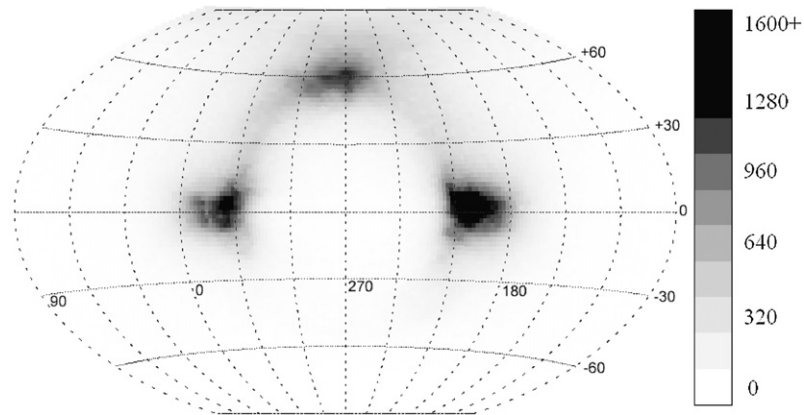
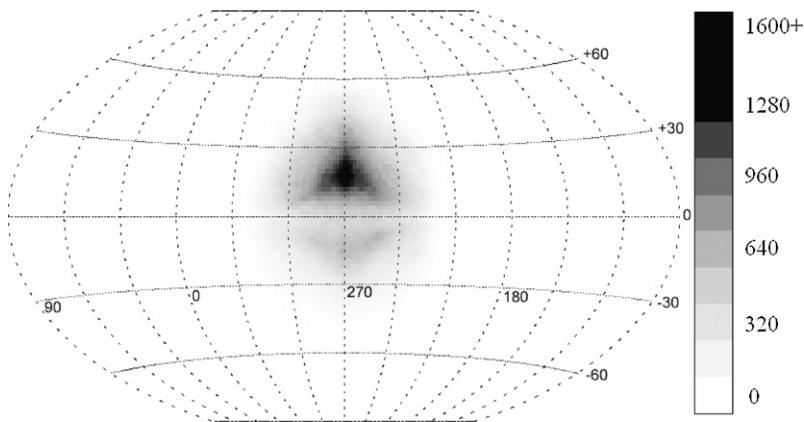Fig. 20. Distribution of prograde orbits, no corrections applied.

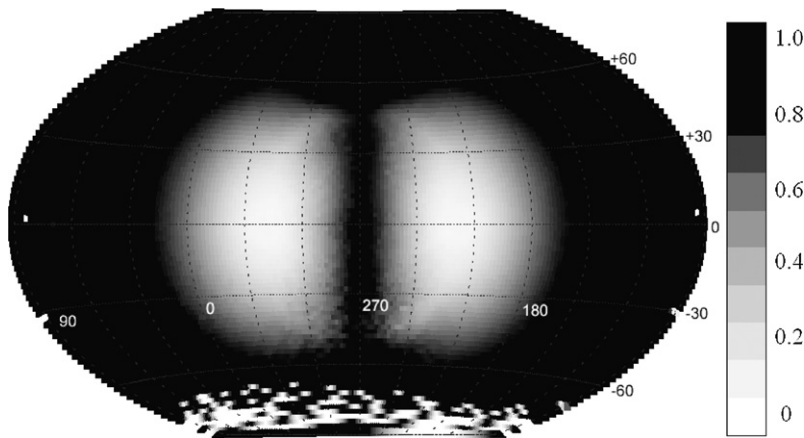Fig. 21. Distribution of retrograde orbits, no corrections applied.

Fig. 22. Perihelion distance of CMOR meteors, in AU.

parent bodies are for each apparent source, how long it takes for meteoroid streams to diffuse into the apparent sporadic sources, and whether the sources are the equilibrium state of a system with equal sources and sinks, or the decaying phase of a sudden infusion of particles at some time in the past.

The origin of most sporadic meteors is thought to be long and short period comets, like those which are parents to meteoroid streams. The streams are thought to lose coherence and gradually evolve to fill the apparent sporadic sources. The

first analysis of meteoroid production and loss mechanisms was done by Whipple (1955), who concluded that comets, particularly Comet 2/P Encke, were important sources of dust in the inner Solar System. Olsson-Steel (1986) has estimated that planetary perturbations are sufficient to move meteoroids from streams to broad apparent sources, and that most meteoroids come from short period comets. On the other hand, Jones et al. (2001) have had good success matching all six apparent sporadic sources using a uniform initial distribution
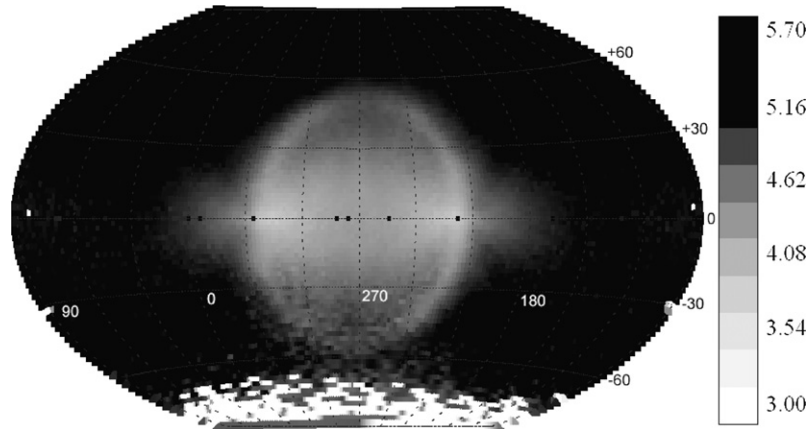
Fig. 23. Log of collisional lifetimes (in years) of CMOR meteors.
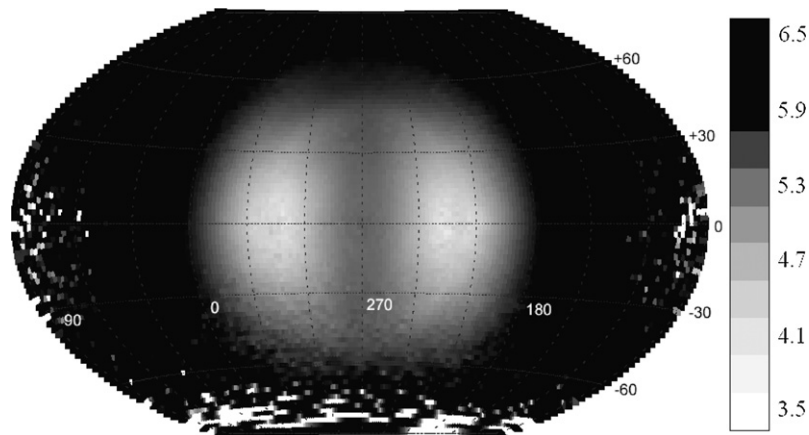

Fig. 24. Log of Poynting–Robertson lifetimes (in years) of CMOR meteors.
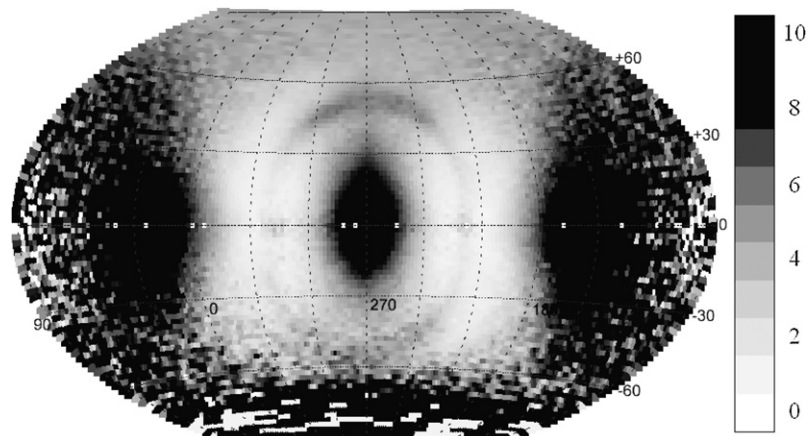

Fig. 25. Ratio of Poynting–Robertson lifetimes to collisional lifetimes of CMOR meteors.

of long and short period comets, and evolving the orbits only with Poynting–Robertson. Both Whipple and Olsson-Steel concluded that the current rate of mass influx to the sporadic meteor complex from comets is not sufficient to produce the observed activity; Olsson-Steel postulates that there must either have been many more comets in the past (10^4 years ago) or that one very large comet broke up and produced much of the sporadic meteoroid population in a single event.

The high resolution radiant maps presented here, with the most complete corrections for observing biases, can be used to compare against models of the evolution of meteoroids in this size range from their parent bodies. One way to proceed would be to select shower meteoroids with radiants in each of the apparent sporadic sources and follow their evolution over thousands or tens of thousands of years (depending on the stability of the orbits) to see what the distribution of meteoroids

(a) Raw data
(b) Corrected and mass weighted
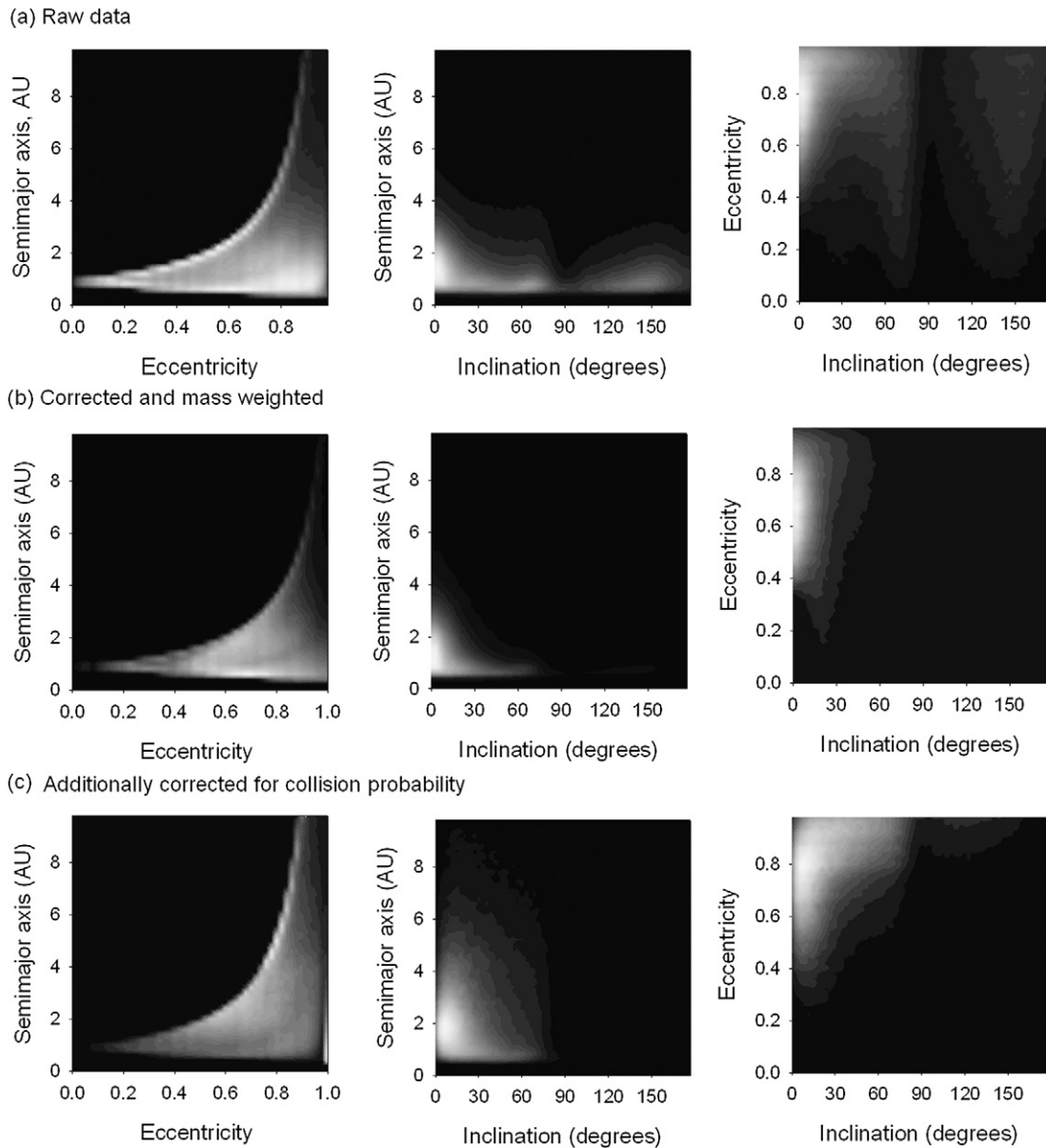(c) Additionally corrected for collision probability

Fig. 26. Distribution of semimajor axis, eccentricity and inclination with respect to each of the other parameters.

approaching the Earth looks like after this time. This should give a good idea of what classes of comets contribute to each of the apparent sources, and how well the current comet distribution can account for the observed sporadic distribution. A complete model must explain the observed triangular shape of the apex sources, and the central component which has low eccentricity and semimajor axis. It should also be able to explain the asymmetry of the north toroidal source.

The ring depleted in radiants is almost certainly due to the shorter collisional lifetimes of retrograde particles inside a ring 55 degrees from the apex. Particles in this region tend to have small semimajor axes, so they travel through regions of relatively high particle density compared to the particles just outside the ring, which have larger *a*'s. Particles just inside the ring also have high inclinations, which means their encounter

speeds tend to be high, so the probability of catastrophic collisions is high compared to low inclination particles with similar orbits. It is very important, when judging whether the current contribution of meteoroids from comets is sufficient to maintain the observed meteoroid population, to take collisional lifetimes (not just Poynting–Robertson) into account. The apex sources in particular are dominated by collisional effects. The fact that the north toroidal source has relatively high lifetimes (both collisional and PR) may explain why the toroidal source is weaker in data at smaller meteoroid masses: the lifetimes may be shorter for smaller meteoroids, producing a skewed mass distribution.

The variation of apparent source strength, location and shape with solar longitude is of great interest, particularly in determining the number and approximate orbits of the parent bodies of

each apparent source. While the CMOR single-station echoes have been carefully calibrated over the last five years, the numbers of orbits depend on the strength of the microwave links from the remote receivers, and this has only been monitored since 2006. In the future, variations over time in the orbital data set will be calibrated against the single station fluxes to obtain true activity profiles for every radiant of the sporadic meteoroid complex.

Acknowledgments

References

Bronshten, V.A., 1983. Physics of Meteoric Phenomena. Reidel, Dordrecht.

Brown, P., Jones, J., 1995. A determination of the strengths of sporadic radio-meteor sources. Earth Moon Planets 68, 223–245.

Brown, P., Weryk, R., Wong, D.K., Jones, J., 2008. A meteoroid stream survey using the Canadian Meteor Orbit Radar I: Methodology and radiant catalogue. Icarus, doi: 10.1016/j.icarus.2007.12.002, in press.

Campbell-Brown, M.D., 2007. Directional variation of sporadic meteor activity and velocity. Earth Moon Planets 102, 79–84.

Ceplecha, Z., Borovička, J., Elford, W.G., Revelle, D.O., Hawkes, R.L., Porubčan, V., Šimek, M., 1998. Meteor phenomena and bodies. Space Sci. Rev. 84, 327–471.

Chau, J.L., Woodman, R.F., Galindo, F., 2007. Sporadic meteor sources as observed by the Jicamarca high-power large-aperture VHF radar. Icarus 188, 162–174.

Cook, A.F., Flannery, M.R., Levy, H., McCrosky, R.E., Sekanina, Z., Shao, C.Y., Southworth, R.B., Williams, J.T., 1972. Meteor research program. Final contract report NSR 09-015-033, NASA CR 2109. Smithsonian Institute, Cambridge, MA.

Elford, W.G., Hawkins, G.S., 1964. Meteor echo rates and the flux of sporadic meteors. Smithsonian Astrophys. Observatory research report No. 9.

Galligan, D.P., Baggaley, W.J., 2004. The orbital distribution of radar-detected meteoroids of the Solar System dust cloud. Mon. Not. R. Astron. Soc. 353, 422–446.

Galligan, D.P., Baggaley, W.J., 2005. The radiant distribution of AMOR radar meteors. Mon. Not. R. Astron. Soc. 353, 422–446.

Hawkins, G.S., 1956. Variation in the occurrence rate of meteors. Astron. J. 61, 386–391.

Jones, J., Brown, P., 1993. Sporadic meteor radiant distributions—Orbital survey results. Mon. Not. R. Astron. Soc. 265, 524–532.

Jones, J., Webster, A.R., Hocking, W.K., 1998. An improved interferometer design for use with meteor radars. Radio Sci. 33, 55–65.

Jones, J., Campbell, M., Nicolova, S., 2001. Modeling of the sporadic meteoroid streams. In: Warmbein, B. (Ed.), Proceedings of Meteoroids 2001. ESA Publications Division, Noordwijk, pp. 575–580.

Jones, J., Brown, P., Ellis, K.J., Webster, A.R., Campbell-Brown, M., Krzemenski, Z., Weryk, R.J., 2005. The Canadian Meteor Orbit Radar: System overview and preliminary results. Planet. Space Sci. 53, 413–421.

Lindblad, B.A., 2001. IAU Meteor Data Center. In: Warmbein, B. (Ed.), Proceedings of Meteoroids 2001. ESA Publications Division, Noordwijk, pp. 71–72.

Morbidelli, A., Gladman, B., 1998. Orbital and temporal distributions of meteorites originating in the asteroid belt. Meteorit. Planet. Sci 33, 999–1016.

Olsson-Steel, D., 1986. The origin of the sporadic meteoroid component. Mon. Not. R. Astron. Soc. 219, 47–73.

Sekanina, Z., 1976. Statistical model of meteor streams. IV. A study of radio streams from the synoptic year. Icarus 27, 265–321.

Steel, D.I., 1996. Meteoroid orbits. Space Sci. Rev. 78, 507–553.

Steel, D.I., Elford, W.G., 1986. Collisions in the Solar System. III. Meteoroid survival times. Mon. Not. R. Astron. Soc. 218, 185–199.

Taylor, A.D., 1995. The Harvard Radio Meteor Project meteor velocity distribution reappraised. Icarus 166, 154–158.

Taylor, A.D., Elford, W.G., 1998. Meteoroid orbital element distributions at 1 AU deduced from the Harvard Radio Meteor Project observations. Earth Planets Space 50, 569–575.

Weiss, A.A., Smith, J.W., 1960. A southern hemisphere survey of the radiants of sporadic meteors. Mon. Not. R. Astron. Soc. 121, 5–16.

Weryk, R.J., Brown, P., 2004. A search for interstellar meteoroids using the Canadian Meteor Orbit Radar (CMOR). Earth Moon Planets 95, 221–227.

Whipple, F.L., 1955. A comet model. III. The zodiacal light. Astrophys. J. 121, 750–770.